JOURNAL OF THEORETICAL AND APPLIED MECHANICS
51, 2, pp. 275-286, Warsaw 2013

ACTIVE VIBRATION CONTROL OF SMART COMPOSITE BEAMS USING PSO-OPTIMIZED SELF-TUNING FUZZY LOGIC CONTROLLER

Nemanja Zorić, Aleksandar Simonović, Zoran Mitrović, Slobodan Stupar
University of Belgrade, Faculty of Mechanical Engineering, Serbia
e-mail: nzoric@mas.bg.ac.rs

This paper presents the optimized fuzzy logic controller (FLC) with on-line tuning of scaling factors for vibration control of thin-walled composite beams. In order to improve the performances and robustness properties of FLC, the proposed method adjusts the input scaling factors via peak observer. The membership functions of the proposed FLC are optimized using the particle swarm optimization (PSO) algorithm. The composite beam is modeled by the third-order shear deformation theory (TSDT) and discretized by using the finite element method. Several numerical examples are provided for the cantilever composite beam under a periodic excitation and periodic excitation with an unexpected disturbance. In order to present the efficiency of the proposed controller, the obtained results are compared with the corresponding results in the cases of the optimized FLCs with constant scaling factors and LQR optimal control strategy.

Key words: optimal vibration control, fuzzy logic control, smart beams

1. Introduction

Thin-walled composite structures are used for aerospace applications such as aircraft wings, wind turbine blades and helicopter blades. The appearance of unwanted vibration may result in instability of the system and, also, can reduce structural life and lead to catastrophic failure. In order to control vibrations of thin-walled structures during operation, conventional structures have been combined with sensing and actuating mechanisms to develop "smart structures" (Gabbert, 2002). In recent years, a great number of researches have been using piezoelectric materials as distributed actuators and sensors (A/Ss) for active vibration control.

The dynamic performance and functionality of smart structures depend on the control algorithm. There are numerous control algorithms which can be applied for vibration suppression of thin-walled structures with distributed piezoelectric A/Ss. The most commonly used control algorithms are "classical" control algorithm such as direct proportional feedback, constant gain velocity feedback (CGVF) and constant amplitude velocity feedback (CAVF) control (Kumar and Narayanan, 2008; Kapuira and Yasin, 2010). Optimal control algorithms (LQR and LQG) for active vibration suppression were adopted by Kumar and Narayanan (2008), Roy and Chakraborty (2009), Kapuira and Yasin (2010) and Gabbert *et al.* (2005).

These control algorithms can provide adequate control managment for wide classes of problems related to active vibration suppression, but they are sensitive to structure characteristics and recquire an exact mathematical model of a structure even for the collocated system. Also, they are sensitive to operating conditions, furthermore, it is difficult to adjust controller gains. An alternative is the use of intelligent control algorithms based on soft computing schemes such as fuzzy logic control (FLC) algorithms. The fuzzy set theory was established by Zadeh (1965) and it has been extensively researched in various fields of engineering. The main advantage of FLC over conventional control approaches is that the FLC is considered artificial intelligence where control laws are designd by human intelligence based on expert's experience, not by a

deterministic numerical calculation. FLC does not recquire the accurate mathematical model of the controlled object and it can represent almost any deterministic controller. Therefore, FLC method has been applied widely for active vibration control of flexible structures (Sharma *et al.*, 2007; Marinaki *et al.*, 2010; Wei *et al.*, 2010).

Fuzzy control design is composed of three important stages. The first stage is the inference rules design, the second is tuning of membership functions, and the third is tuning of control parameters. This paper deals with active vibration control of smart composite beams using an optimized self-tuning fuzzy logic controller (FLC). Input variables in FLC are scaled with scaling factors, and, in order to improve the performance and robustness properties of FLC, these scaling factors are adjusted via peak observer. The membership functions of the proposed FLC are optimized using the particle swarm optimization (PSO) algorithm. The composite beam is modeled by the third-order shear deformation theory (TSDT) and discretized using the finite element method. Numerical examples are provided for the cantilever composite beam under a periodic excitation and a periodic excitation with unexpected disturbance. The results obtained using the proposed self-tuning FLC are then compared with the corresponding results in the cases of PSO-optimized FLC with constant scaling factors and LQR optimal control strategy.

2. Governing equations

2.1. Coupled equations of motion

The laminated composite beam with integrated piezoelectric actuators and sensors considered here is presented in Fig. 1. Both elastic and piezoelectric layers are supposed to be thin, so a plane stress state can be assumed. The sensors and actuators are perfectly bonded on the upper and lower surfaces at different locations along the length of the beam. It is assumed that they span the entire width of beam. The elastic layers are obtained by setting their piezoelectric coefficients to zero. A single mechanical displacement field is considered for all layers while electric displacements are considered for each layer independently.

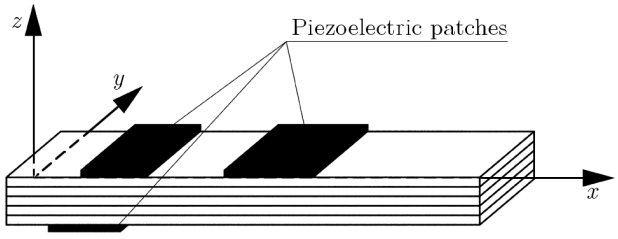

Fig. 1. Composite beam with integrated piezoelectric layers

The beam is discretized using the finite element method based on the third-order shear deformation theory (Heyliger and Reddy, 1985). The formulation results in a coupled finite element model with mechanical (displacements) and electrical (potentials of piezoelectric patches) degrees of freedom (Zorić *et al.*, 2012)

$$\boldsymbol{M}\ddot{\mathbf{u}} + \mathbf{C}_d\dot{\mathbf{u}} + \mathbf{K}^*\mathbf{u} = \mathbf{F}_m - (\mathbf{K}_{me})_A\boldsymbol{\phi}_{AA} \tag{2.1}$$

where $\mathbf{u}$ presents the vector of generalized mechanical displacmenets, $\boldsymbol{M}$ presents the mass matrix, $(\mathbf{K}_{me})_A$ is the piezoelectric stiffness matrix of the actuator, $\mathbf{C}_d$ is the damping matrix, $\boldsymbol{\phi}_{AA}$ is the vector of external applied voltage on the actuators, $\mathbf{F}_m$ is the vector of external forces and $\mathbf{K}^*$ is the coupled stiffness matrix given as

$$\mathbf{K}^* = \mathbf{K}_m + (\mathbf{K}_{me})_A(\mathbf{K}_e)_A^{-1}(\mathbf{K}_{me})_A^{\mathrm{T}} + (\mathbf{K}_{me})_S(\mathbf{K}_e)_S^{-1}(\mathbf{K}_{me})_S^{\mathrm{T}} \tag{2.2}$$

where $\mathbf{K}_m$ presents the elastic stiffness matrix, $(\mathbf{K}_{me})_S$ is the piezoelectric stiffness matrix of the sensor and $(\mathbf{K}_e)_A$ and $(\mathbf{K}_e)_S$ are the dielectric stiffness matrices of the actuator and sensor, respectively.

2.2. Modal analysis

For practical implementation, the obtained model needs to be truncated, where only the first few modes are taken into account. Thus, the displacement vector can be approximated by the modal superposition of the first r modes as

$$\mathbf{u} \approx \boldsymbol{\Psi}\boldsymbol{\eta} \tag{2.3}$$

where $\boldsymbol{\Psi}$ presents the modal matrix, and $\boldsymbol{\eta}$ the vector of modal coordinates. Using Equation (2.3), Equation (2.1) can be transformed in the reduced modal space as

$$\ddot{\boldsymbol{\eta}} + \boldsymbol{\Lambda}\dot{\boldsymbol{\eta}} + \boldsymbol{\omega}^2\boldsymbol{\eta} = \boldsymbol{\Psi}^{\mathrm{T}}\mathbf{F}_m - \boldsymbol{\Psi}^{\mathrm{T}}(\mathbf{K}_{me})_A\boldsymbol{\phi}_{AA} \tag{2.4}$$

where $\boldsymbol{\omega}^2$ presents the diagonal matrix of the squares of the natural frequencies, and

$$\boldsymbol{\Lambda} = \operatorname{diag}_{i=1,r}(2\zeta_i\omega_i) \tag{2.5}$$

presents the modal damping matrix in which ζ_i is the natural modal damping ratio of the i-th mode.

2.3. State-space representation

Equation (2.4) can be expressed in the state-space form as

$$\dot{\mathbf{X}} = \mathbf{A}\mathbf{X} + \mathbf{B}\boldsymbol{\phi}_{AA} + \mathbf{d} \tag{2.6}$$

where

$$\begin{aligned} &\mathbf{X} = \begin{Bmatrix} \eta \\ \dot{\eta} \end{Bmatrix} \qquad \mathbf{A} = \begin{bmatrix} \mathbf{0} & \mathbf{I} \\ -\boldsymbol{\omega}^2 & -\boldsymbol{\Lambda} \end{bmatrix} \\ &\mathbf{B} = \begin{bmatrix} \mathbf{0} \\ \overline{\mathbf{B}} \end{bmatrix} = \begin{bmatrix} \mathbf{0} \\ -\boldsymbol{\Psi}^{\mathrm{T}}(\mathbf{K}_{me})_A \end{bmatrix} \qquad \mathbf{d} = \begin{bmatrix} \mathbf{0} \\ \boldsymbol{\Psi}^{\mathrm{T}}\mathbf{F}_m \end{bmatrix} \end{aligned} \tag{2.7}$$

present the state vector, the system matrix, the control matrix disturbance respectively, where $\mathbf{I}$ and $\mathbf{0}$ are the appropriately dimensioned identity and zero matrix. The sensor output equation can be written as

$$\mathbf{Y}_S = \mathbf{C}_S\mathbf{X} \tag{2.8}$$

where $\mathbf{C}_S$ presents the output matrix which depends on the modal matrix and sensor piezoelectric stifeness matrix.

3. Fuzzy logic control

3.1. Design of the fuzzy logic controller

The idea of fuzzy logic control (FLC) is using linguistic directions as a basis for control. By incorporating human expertise into the fuzzy IF-THEN rules, FLC can be embedded into a

closed-loop system, similarly to conventional controllers. The most used fuzzy control inference is the Mamdani fuzzy inference, whose i-th rule can be written as follows

$$R^i: \quad \mathrm{i}f \quad I_1 = A_i \quad \wedge \quad I_2 = B_i \quad \text{then} \quad O = C \tag{3.1}$$

where I_1 and I_2 present the input variables, O is the output variable, and A_i, B_i and C_i are the linguistic values of the fuzzy variables. In general, FLC consists of four principal elements: fuzzification, rule base, decision making and defuzzification.

The first stage in building the fuzzy controller is choosing input/output parameters. Two commonly input variables are the error and the error derivative. In this study, the inputs are modal displacement η and its time derivative-modal velocity $\dot{\eta}$. The output variable is control voltage applied on the actuator ϕ_{AA}. The fuzzy logic controller uses crisp data directly from the sensor. These are converted into linguistic values through the fuzzification process. Each input and output fuzzy variable is defined in the fuzzy space in the form of five linguistic variables namely NB (negative big), NS (negative small), ZE (zero), PS (positive small) and PB (positive big). In this study, the trapezoid membership function is used to present NB and PB variables and the triangular membership function to present NS, ZE and PB variables. The universes of discourse of the inputs and the output are set to be $[-1, 1]$, hence, the inputs need to be scaled, thus its minimum value be -1, and maximum 1. The scaling of the inputs is performed on the following way

$$E = K_d\eta \qquad EC = K_v\dot{\eta} \tag{3.2}$$

where E and EC present the error and the error derivative in the fuzzy set, and K_d and K_v present the displacement and the velocity scaling factor, respectively. Also, the output from the fuzzy set needs to be scaled in the following way

$$\phi_{AA} = K_{act}U \tag{3.3}$$

where U presents the output from the fuzzy set, and K_{act} is the output scaling factor which is equal to the maximum allowable voltage which can be applied to the piezoelectric actuator. The membership functions of the inputs and the output are presented in Fig. 2. The membership functions are parameterized by parameters presented by the matrix $\boldsymbol{\alpha}$, which are depicted in Fig. 2.

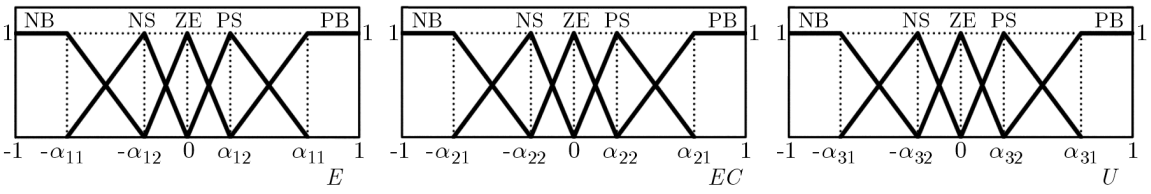

Fig. 2. Membership functions of the inputs and the output

Observing Equation (3.1), and considering the number of fuzzy linguistic variables for each input and output, it can be concluded that the number of fuzzy inference rules is 25. They are presented in a marix form shown in Table 1. For example, the rule described by the second row and second column in Table 1 reads: "IF E is NS and EC is NS, THEN U is PS".

The results of fuzzy inference have to be transformed into a numerical output value through the process of defuzzification. In this study, the center average (centroid) defuzzification method is used. Determination of parameters of the membership functions requires expert knowledge. No fixed process for determination of these parameters exists. In this study, these parameters are optimized in order to maximize control performances.

Table 1. Inference rules used in the proposed FLC

		EC				
		NB	NS	ZE	PS	PB
E	NB	PB	PB	PB	PS	PS
	NS	PS	PS	PS	ZE	ZE
	ZE	PS	PS	ZE	NS	NS
	PS	ZE	ZE	NS	NS	NS
	PB	NS	NS	NB	NB	NB

3.2. Self-tuning fuzzy logic controller

Since the universes of discourse of the input variables are in the range $[-1, 1]$, the scaling factors K_d and K_v have to be chosen in such a way that they transform the input variables from the sensor to the fuzzy controller to be in the range $[-1, 1]$. According to that, the scaling factors for modal displacement and modal velocity can be calculated as follows

$$K_d = \frac{1}{|\eta_{max}|} \qquad K_v = \frac{1}{|\dot{\eta}_{max}|} \tag{3.4}$$

where η_{max} and $\dot{\eta}_{max}$ present the amplitudes of modal displacement and modal velocity. The amplitude is a time varying value and, also, the external excitations which cause vibration have a stochastic nature. Because of that, it is difficult to determine these factors off-line, and keeping them constant through active vibration suppression leads to a decrease of control performances (Wilson, 2005). Qiao and Mizumoto (1996) proposed the tuning of the parameters using peak observer for PID-type FLC. The peak observer, proposed by Qiao and Mizumoto (1996), keeps watching the system output and transmits a signal at each peak, and measures the apsolute peak. In this study, this approach is adapted to the problems of vibration reduction, so, the peak observer is constructed for each input variable in the fuzzy controller. Beside that, the peak observer is modified and, beside watching the peaks, the presented observer also monitors the increase in the ampliude. A block diagram of the self-tuning FLC is presented in Fig. 3.

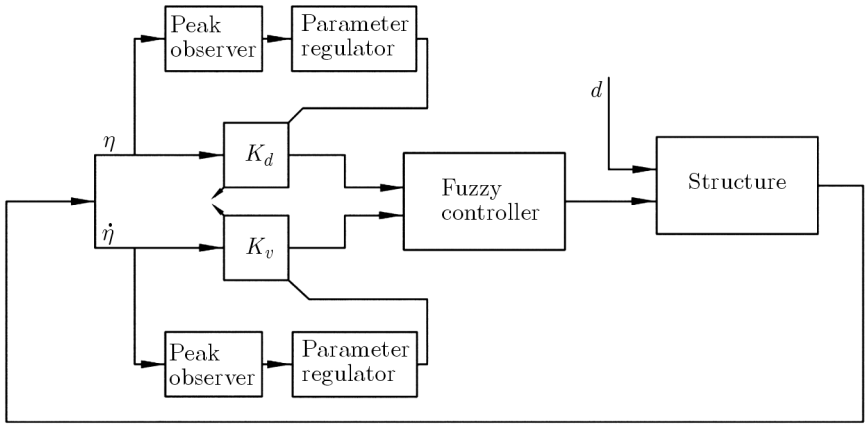

Fig. 3. Block diagram of self-tuning FLC

The presented peak observer monitors the input, and calulates the rates of the input. Considering the k-th sampling time, the current and previous rates of the modal displacement are

$$\Delta\eta(k) = \eta(k) - \eta(k-1) \qquad \Delta\eta(k-1) = \eta(k-1) - \eta(k-2) \tag{3.5}$$

and the displacement scaling factor is tuned in the parameter regulator according to the following expression

$$K_d(k) = \begin{cases} \dfrac{1}{|\eta(k-1)|} & \text{for} \quad \Delta\eta(k)\,\Delta\eta(k-1) \leqslant 0 \\ \dfrac{1}{|\eta(k)|} & \text{for} \quad \Delta\eta(k)\,\Delta\eta(k-1) > 0 \quad \text{and} \quad |\eta(k)| > \dfrac{1}{K_d(k-1)} \\ K_d(k-1) & \text{other} \end{cases} \tag{3.6}$$

For tuning of the velocity scaling factor, the same procedure as for tuning of the displacement scaling factor can be applied. Figure 4 illustratively presents how the scaling factors are tuned via the peak observer.

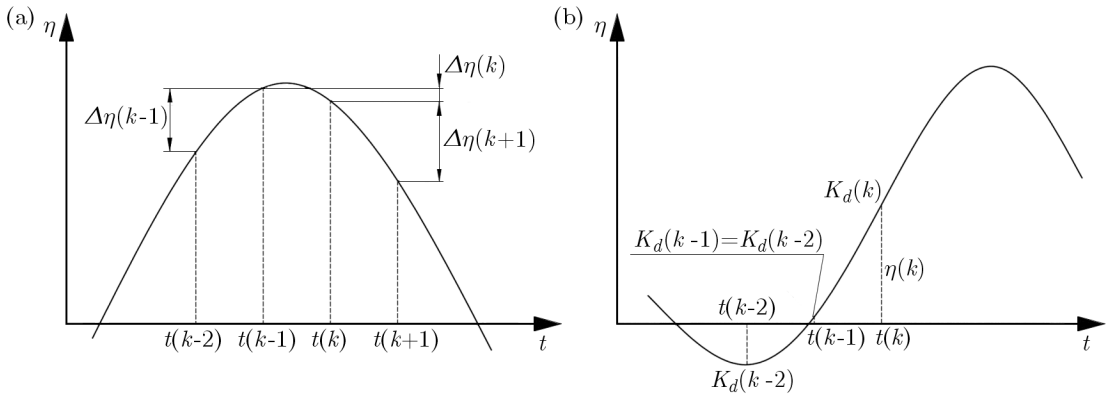

Fig. 4. Tuning of the displacement scaling factor via peak observer

Considering Fig. 4a, it can be seen that $\Delta\eta(k-1) > 0$ and $\Delta\eta(k) < 0$, thus, $\eta(k-1)\eta(k) < 0$, and according to Equation (3.6), the displacement scaling facor is scaled according to this Equation. On the other hand, considering the $(k+1)$-th sampling time, it is obvious that $\Delta\eta(k+1) < 0$, and $\eta(k-1)\eta(k) > 0$, so the displacement scaling factor, in the $(k+1)$-th sampling time, does not change its current value. During operation, a structure can be affected by various disturbances, so, amplitude will be increased. In this case, the scaling factors have to be tuned. This is given by the second row in Equation (3.6) and illustrated in Fig. 4b. Considering Fig. 4b, it can be seen that $\Delta\eta(k-1) > 0$ and $\Delta\eta(k) > 0$, so their product is a positive value, but the absolute value of amplitude in the current, k-th, sampling time $\eta(k)$ is larger than the absolute value of the last peak $\eta(k-2)$. In this case, the displacement scaling factor needs to be tuned so that the input in FLC be in the range $[-1, 1]$.

3.3. Optimization criteria

The next step in designing of FLC is the determination of parameters of the membership functions. In this study, the membership functions are parameterized with parameters presented by the matrix $\boldsymbol{\alpha}$. The aim is to find optimal values of these parameters such that the active vibration suppression is improved. In order to improve the control performances of FLC, the optimization problem can be written as follows

$$\max J = \frac{1}{\|\eta\|} \tag{3.7}$$

where J presents the objective function which has to be maximized, and $\|\eta\|$ presents L^2 norm of the vector of modal displacement. Constraints of this optimization problems are

$$\text{Subject to} \quad \begin{array}{lll} 0 < \alpha_{i,j} \leqslant 1 & i = 1, \ldots, 3 & j = 1, 2 \\ \alpha_{i,2} < \alpha_{i,1} & i = 1, \ldots, 3 & \end{array} \tag{3.8}$$

Incorporating constraints into the optimization problem, the objective function can be transformed as

$$J = \begin{cases} \dfrac{1}{\|\eta\|} & \text{if constraints are not violated} \\ 0 & \text{if constraints are violated} \end{cases} \tag{3.9}$$

4. Optimization implementation using particle swarm optimization technique

The particle swarm optimization (PSO) has been inspired by the social behavior of animals such as fish schooling, insect swarming and birds flocking. It was introduced by Kennedy and Everhart (1995). The system is initialized with a population of random solutions (called particles). Each particle represents a potential solution of the problem, and it is treated as a point in a m-dimensional space. For a given i-th particle, its position is represented as $(p_i) = (p_{i1}, p_{i2}, \ldots, p_{id}, \ldots, p_{i,m})$ in which every coordinate presents a parameter which has to be optimized, and m presents the number of these parameters. The current position of every particle is affected by three factors: its own velocity: $(v_i) = (v_{i1}, v_{i2}, \ldots, v_{id}, \ldots, v_{i,m})$, the best position it has achieved (best local position) which is determined by the highest value of the objective function encountered by this particle in all its previous iteration and overall best position achieved by all particles (best global position), which is determined by the highest value of the objective function encountered in all the previous iteration. The particle changes its velocity and position in the following way

$$\begin{aligned} &v_{id}^{k+1} = \chi v_{id}^k + c_1 r_1 (l_{id} - p_{id}^k) + c_2 r_2 (g_d - p_{id}^k) \\ &p_{id}^{k+1} = p_{id}^k + v_{id}^{k+1} \qquad i = 1, \ldots, n \qquad d = 1, \ldots, m \end{aligned} \tag{4.1}$$

where χ is the inertia weight, c_1 is the cognition factor, c_2 is the social learning factor, r_1 and r_2 are random numbers between 0 and 1, the superscript k denotes the iterative generation, n is the population size, l_{id} and g_d are the best local and the best global position. The cognition and social learning factors are usually set as $c_1 = c_2 = 1.5$. In this study, the coordinates of particles are the parameters given by the matrix $\boldsymbol{\alpha}$.

5. Numerical studies

In this example, a cantilever symmetric laminated beam is considered. The length of the beam is 0.5 m, and its width is 0.025 m. The beam is made of eight graphite-epoxy (carbon-fiber reinforced) layers. The thickness of each layer is 0.25 mm and orientations are $(90^\circ/0^\circ/90^\circ/0^\circ)_S$. The piezoelectric actuator and sensor are made of PZT. Their thicknesses are 0.2 mm, and lengths are 50 mm. The actuator and sensor are placed at the root of the beam and they are collocated. The allowable electric field of piezoceramic materials is around 500-1000 V/mm. Since the thickness of the actuator is 0.2 mm, the maximum allowable voltage has been taken as 200 V. Material properties of the graphite-epoxy layer and PZT are given in Table 2.

The beam is discretized with 50 finite elements, and it is subjected to a periodic loading of $0.02\sin(20t)$ N at the tip. Only the first mode is considered. The number of randomly generated particles is 100, and number of iteration is 100. The inertia weight is lineary varied from 1 to 0.5 through iterations. The cognition and social learning factors in the PSO algorithm are set as $c_1 = c_2 = 1.5$. The initial values of displacement and velocity scaling factors for self-tuning FLC are: $K_d = 10000$ and $K_v = 10$. During simulation, the sampling time is set to be 1 ms, and only the first mode is considered. The natural modal damping ratio is set to be 0.2%. The

obtained results for self-tuning FLC after optimization is presented in Table 3. Figure 5 presents the obtained membership functions. The tip displacement history is depicted in Fig. 6.

Table 2. Material properties of graphite-epoxy and PZT

Material properties	Graphite-Epoxy	PZT
Modulus of elasticity, Y_1 [GPa]	174	63
Modulus of elasticity, Y_2 [GPa]	10.3	63
Shear modulus, G_{13} [GPa]	7.17	24.6
Shear modulus, G_{23} [GPa]	6.21	24.6
Poisson's ratio, ν_{12}	0.25	0.28
Density, ρ [kg/m^3]	1389.23	7600
Piezoelectric constant, e_{31} [C/m^2]	–	10.62
Permittivity constant, k_{33} [F/m]	–	$15.55 \cdot 10^{-9}$

Table 3. Initial displacement and velocity scaling factors, parameter matrix, objective function value and maximim applied voltage for self-tuning FLC obtained by PSO

K_d	K_v	$\boldsymbol{\alpha}$	J	Max. actuator voltage [V]
10000	10	$\begin{bmatrix} 0.056 & 0.028 \\ 0.06 & 0.03 \\ 0.92 & 0.46 \end{bmatrix}$	$1.11 \cdot 10^4$	164.5

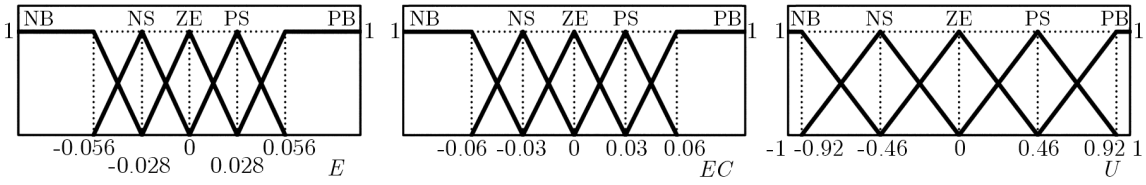

Fig. 5. Membership functions for the inputs and output of the self-tuning FLC optimized by PSO

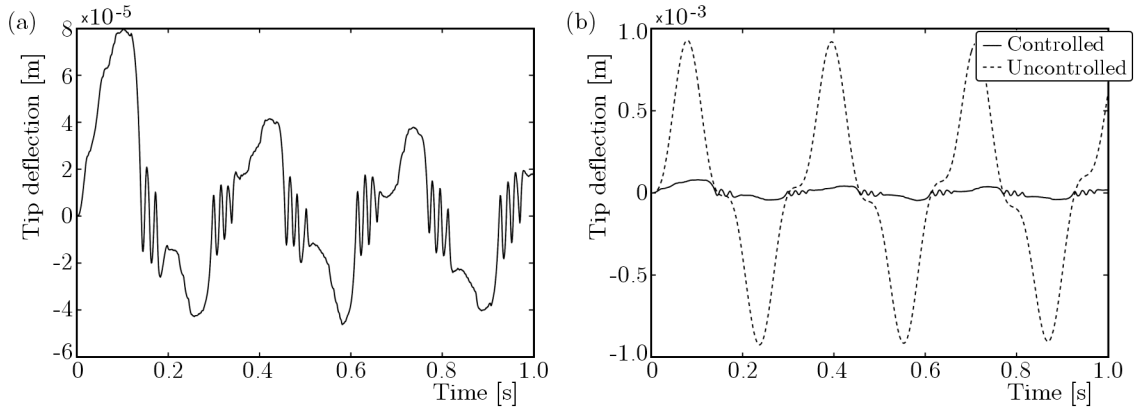

Fig. 6. Tip displacement history: (a) self-tuning FLC optimized by PSO, (b) comparison of self-tuning FLC optimized by PSO with uncontrolled tip displacement

In order to present the influence of initial settings of the scaling factors K_d and K_v and performances of the controller optimized for the specific initial scaling factors with different initial factors used, the numerical simulation is performed with the following initial values:

$K_d = 0$, $K_v = 0$ and $K_d = 1000$, $K_v = 10$. Tip displacement histories for different initial values of the factors are depicted in Fig. 7a. From Fig. 7a, it can be concluded that different initial values of the scaling factors affect only the first 0.3 s of vibration suppression. After that, these factors are adjusted, and the control performances do not differ from the initial values of scaling factors which were used for optimization.

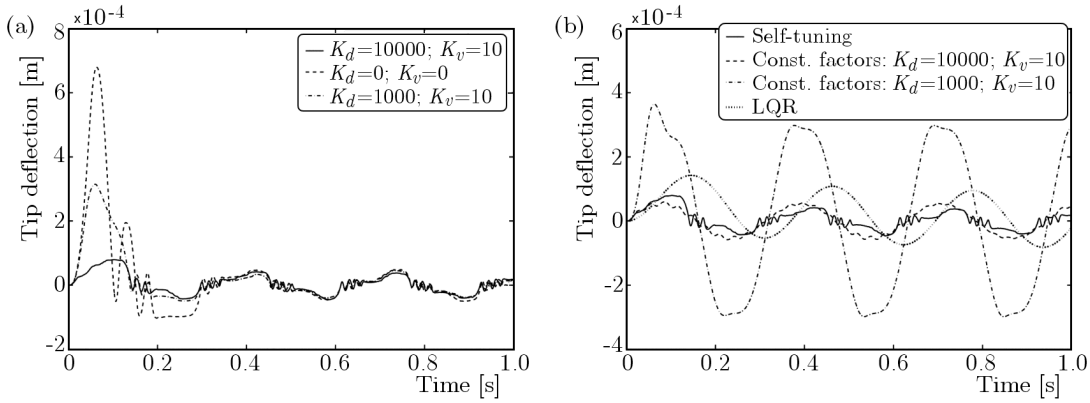

Fig. 7. Tip displacement histories: (a) for different initial values of scaling factors, (b) comparison self-tuning FLC with FLC with constant factors and LQR optimal control

The next aim is the comparison of the presented optimized self-tuning FLC with the optimized FLC having constant scaling factors and optimal LQR. For this purpose, the membership functions of FLC with constant factors are optimized with the proposed optimization technique for two examples considering the same loading as in the self-tuning FLC. In the first example, the scalling factors are set to be $K_d = 10000$ and $K_v = 10$, and in the second example: $K_d = 1000$ and $K_v = 10$. The obtained results are presented in Table 4. For optimal LQR control, the weighting matrices $\mathbf{Q}$ and $\mathbf{R}$ are obtained by a trial and error solution, and the reuslts are presented in Table 5. The tip deflection histories are depicted in Fig. 7b.

Table 4. Displacement and velocity scaling factors, parameter matrix, objective function value and maximim applied voltage for FLC with constant scaling factors obtained by PSO

	K_d	K_v	$\boldsymbol{\alpha}$	J	Max. actuator voltage [V]
First example	10000	10	$\begin{bmatrix} 0.05 & 0.025 \\ 0.86 & 0.43 \\ 0.764 & 0.382 \end{bmatrix}$	$9.11 \cdot 10^3$	155.5155
Second example	1000	10	$\begin{bmatrix} 0.056 & 0.028 \\ 0.06 & 0.03 \\ 0.92 & 0.46 \end{bmatrix}$	$1.53 \cdot 10^3$	97.151

Table 5. Matrices $\mathbf{Q}$ and $\mathbf{R}$ and maximum control voltage for LQR optimal control

$\mathbf{Q}$	$\mathbf{R}$	Max. actuator voltage [V]
$10^{12}\mathbf{I}_{2\times 2}$	1	170

From Fig. 7b, it can be concluded that the proposed self-tuning FLC is more efficient in active vibration suppression than the classic FLC with constant scaling factors and LQR optimal control. Comparing the maximum voltage obtained in the self-tuning FLC (see Table 3) and the maximum voltage obtained in LQR (see Table 5), it is evident that, beside better efficiency in active vibration suppression, the self-tuning FLC provides a little less maximum applied voltage than LQR.

Furthermore, in order to investigate the robustness of the self-tuning FLC optimized PSO and its ability to work for different loadings, the obtained parameters for a specific loading is used for differential loadings. In other words, the parameters obtained by using PSO for loading $0.02\sin(20t)$, are applied when the loadings are equal $0.02\sin(10t)$, $0.02\sin(30t)$ and $0.02\sin(40t)$. The tip displacement histories for different loadings are presented in Fig. 8. From Fig. 8, it can be concluded that the proposed controller, that is optimized for one loading, can be applied successfully when other loadings are used.

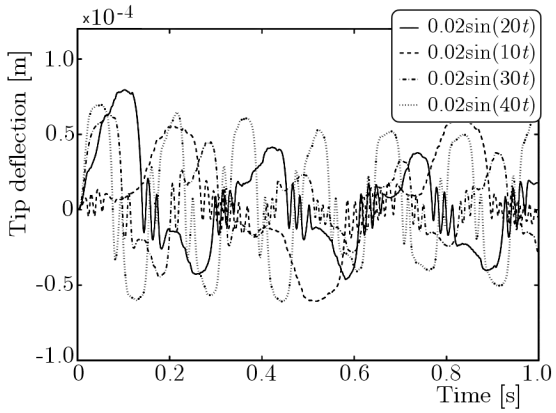

Fig. 8. Tip displacement histories of self-tuning FLC for different loadings

The next study about robustness of the proposed FLC is carried out under a periodic excitation with unexpected disturbance. The tip of the beam is subjected to the periodic loading of $0.02\sin(20t)$ N, and in 0.5 s, the unexpected disturbance of 1 N with duration of 1 ms is applied. The response of the self-tuning FLC is compared with the responses of FLCs with constant scaling factors and LQR optimal control.

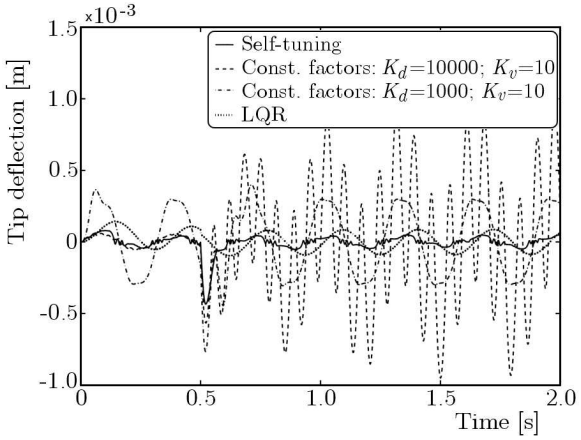

Fig. 9. Tip displacement histories for a harmonic loading with unexpected disturbance

The tip displacement histories are plotted in Fig. 9. Histories of the applied control voltages for the self-tuning FLC and LQR are depicted in Fig. 10. Observing Fig. 9, it can be concluded that the performances of the self-tuning FLC and of LQR are not significantly affected. For the

first example of the FLC with constant factors ($K_d = 10000$, $K_v = 10$), it can be seen form Fig. 9 that, after appearing of the unexpected disturbance, the amplitude is significantly increased. On the other hand, comparing the applied control voltages during active vibration suppression for the self-tuning FLC and LQR, given in Fig. 10, it is evident that in the case of LQR, the maximum applied voltage is drastically increased, near 2000 V. In this case, depolarization of the piezoelectric actuator is inevitable.

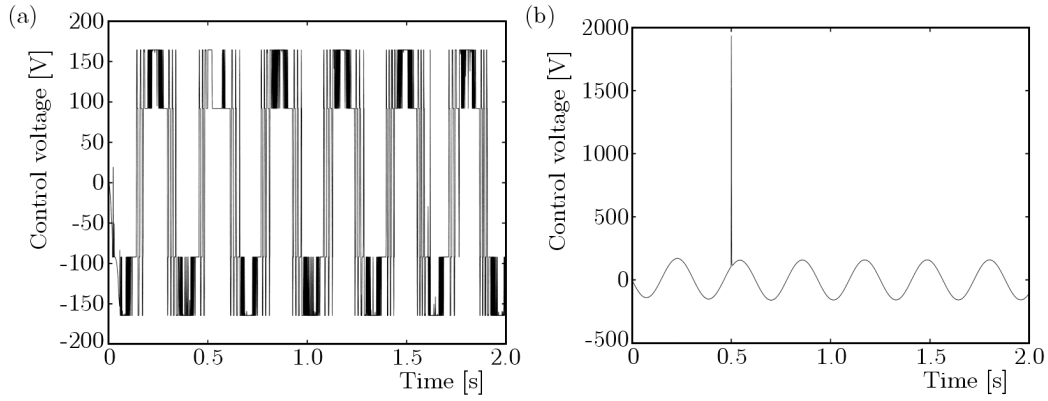

Fig. 10. Histories of the applied control voltage; (a) self-tuning FLC, (b) LQR

6. Conclusions

This paper presents active vibration control of smart composite beams using PSO-optimized self-tuning FLC. Input variables in FLC are scaled with scaling factors, and, in order to improve the performance and robustness of FLC, these scaling factors are adjusted via peak observer. The membership functions of the proposed FLC are optimized using the Particle swarm optimization (PSO) algorithm.

Taking into account several numerical examples performed for the cantilever composite beam, where the PSO-optimized self-tuning FLC is compared with PSO-optimized FLCs with constant factors and the LQR control algorithm, one finds that the PSO-optimized self-tuning FLC is much more effective in vibration control than other investigated control algorithms.

Although the proposed optimized self-tuning FLC is applied to the beam in the case of the first mode response, taking into consideration all advantages presented here, this technique can be applied to more complex structures like plates and shells, and for multimodal responses.

Acknowledgment

This work is supported by the Ministry of Science and Technological Development of the Republic of Serbia through Technological Development Projects No. 35035 and No. 35006.

References

1. Gabbert U., 2002, Research activities in smart materials and structures and expectations to future developments, *Journal of Theoretical and Applied Mechanics*, **40**, 3, 549-574

2. Gabbert U., Nestorović-Trajkov T., Köppe H., 2005, Controller design and implementation for active vibration suppression of a piezoelectric smart shell structure, *Journal of Theoretical and Applied Mechanics*, **43**, 3, 487-500

3. Heyliger N.D., Reddy N., 1985, A higher order beam finite elements for bending and vibration problem, *Journal of Sound and Vibration*, **126**, 309-326

4. Kaipura S., Yasin M.Y., 2010, Active vibration suppression of multilayered plates integrated with piezoelectric fiber reinforced composites using an efficient finite element model, *Journal of Sound and Vibration*, **329**, 3247-3265

5. Kennedy J., Everhart R.C., 1995, Particle swarm optimization, *Proceedings of the IEEE International Conference on Neural Networks*, **4**, 1942-1948

6. Kumar R.K., Narayanan S., 2008, Active vibration control of beams with optimal placement of sensor/actuator pairs, *Smart Materials and Structures*, **17**

7. Marinaki M., Marinakis M., Stavroulakis G.E., 2010, Fuzzy control optimized by PSO for vibration suppression of beams, *Control Engineering Practice*, **18**, 618-629

8. Qiao W.Z., Mizumoto M., 1996, PID tupe fuzzy controller and parameters adaptive method, *Fuzzy Sets and Systems*, **78**, 1, 23-35

9. Roy T., Chakraborty D., 2009, Optimal vibration control of smart fiber reinforced composite shell structures using improved genetic algorithm, *Journal of Sound and Vibration*, **319**, 15-40

10. Sharma M., Singh S.P., Sachdeva B.L., 2007, Modal control of a plate using a fuzzy logic controller, *Smart Materials and Structures*, **16**, 1331-1341

11. Wei J., Qiu Z., Han J., Wang Y., 2010, Experimental comparison research on active vibration control for flexible piezoelectric manipulator using fuzzy controller, *Journal of Intelligent and Robotic Systems*, **59**, 31-56

12. Wilson C.M.D., 2005, *Fuzzy Control of Magnetorheological Dampers for Vibration Reduction of Seismically Excited Structures*, Ph.D.Thesis, Florida State University, Tallahassee

13. Zadeh L.A., 1965, Fuzzy sets, *Information and Control*, **8**, 338-353

14. Zorić N., Simonović A., Mitrović Z., Stupar S., 2012, Multi-objective fuzzy optimization of sizing and location of piezoelectric actuators and sensors, *FME Transactions*, **40**, 1-9

Aktywna redukcja drgań „inteligentnych" belek kompozytowych za pomocą samostrojącego sterownika z logiką rozmytą i zoptymalizowanego metodą PSO

Streszczenie

W pracy zaprezentowano zoptymalizowany sterownik z logiką rozmytą (FLC) o bieżąco dostrajanych współczynnikach skalowania zastosowany do redukcji drgań cienkościennych belek kompozytowych. Dla poprawy efektywności i stabilności pracy sterownika zaproponowano dostrajanie współczynników skalowania na wejściu poprzez śledzenie wartości szczytowej sygnału. Funkcje przynależności sterownika FLC zoptymalizowano algorytmem roju cząstek (PSO). Rozważaną belkę kompozytową opisano modelem teorii odkształceń postaciowych trzeciego rzędu (TSDT) i zdyskretyzowano metodą elementów skończonych. Przedstawiono kilka przykładów belki wspornikowej poddanej wymuszeniu okresowemu z nieoczekiwanym zakłóceniem tego wymuszenia. W celu zeprezentowania efektywności analizowanego sterownika uzyskane wyniki porównano z istniejącymi rezultatami odpowiadającymi sterownikom FLC o stałych współczynnikach skalowania i zoptymalizowanej strategii sterowania wykorzystującej regulator liniowo-kwadratowy (LQR).

Manuscript received April 11, 2012; accepted for print May 24, 2012